The Discovery of Halley-sized Kuiper Belt Objects Using HST

Anita L. Cochran[1]
Astronomy Department & McDonald Observatory, University of Texas, Austin, TX 78712

Harold F. Levison[1] and S. Alan Stern[1]
Geophysical, Astrophysical, & Planetary Sciences, Southwest Research Institute,
1050 Walnut St, Suite 429, Boulder, CO 80302

Martin J. Duncan[1]
Physics Department, Queens University, Kingston, Ontario K7L 3N6

ABSTRACT

We report the statistical detection (at the $> 99\%$ confidence level) of a population of 28th magnitude objects exhibiting proper motions of $\approx$1 arcsecond per hour at quadrature in deep HST/WFPC2 images. The drift directions imply a preponderance of objects on prograde orbits concentrated near the ecliptic plane. We interpret this as the detection of objects which reside in the Kuiper belt near or beyond the orbit of Neptune, comparable in size to comet 1P/Halley (radii ~ 10 KM for an albedo of 4%). Our observations imply a population of $\sim 2.5 \times 10^4$ objects deg^{-2} with $V < 28.6$. This must be viewed as a lower limit until our search of parameter space is complete. Our observations imply that there are $> 2 \times 10^8$ objects of this size in the Kuiper belt with inclinations $< 12°$ and within ~ 40 AU of the Sun.

Subject headings: comets: general – solar system: formation – solar system: general

1. Introduction

[1]Based on observations with NASA/ESA Hubble Space Telescope obtained at the Space Telescope Science Institute, which is operated by Universities for Research in Astronomy, Incorporated, under NASA contract NAS5-26555.

Recently, over 20 objects with radii of 100–200 KM have been discovered beyond the orbit of Neptune that may represent the brightest members of a heretofore undetected class of objects in the solar system (Jewitt & Luu 1995; also Stern 1995, Weissman 1995). Such a population has been suspected since Edgeworth (1949) and Kuiper (1951) independently pointed out that it seems unlikely that the disk of planetesimals that formed the planets would have abruptly ended at the edge of the planetary system, and that originally there was a significant number of planetesimals (*i.e.* comets) in near-circular orbits outside the planetary region.

Fernandez (1980) suggested that such a belt of distant icy planetesimals could serve as the source of the short-period comets and would be more dynamically efficient than evolving long-period comets inward from the Oort cloud as first suggested by Newton (1893; also Everhart 1972, 1977). Duncan *et al.* (1988) confirmed this with dynamical simulations which showed that a cometary source with a low initial inclination distribution was far more consistent with the observed orbits of the short-period comets than the randomly distributed inclinations of comets in the Oort cloud. Subsequent numerical integrations have shown that a significant fraction of the objects that formed in the Kuiper belt are stable for the age of the solar system but that weak gravitational instabilities provide a large enough influx to replenish the current population of short-period comets if the population of the Kuiper belt region is $\sim 10^{10}$ objects (Levison & Duncan 1993, Holman & Wisdom 1993, Duncan *et al.* 1995). However, the detection of objects the size of short-period comets in the Kuiper belt, which is necessary to confirm these predictions, has been beyond observational reach until very recently. The theoretical work referred to above did, however, spur searches for larger objects. Such objects were first discovered in 1992 (Jewitt & Luu 1992). As of this writing, 24 such objects have been discovered. Of these, 11 have been observed over a long enough period of time to have fairly well determined orbits (Marsden, priv. comm.). All 11 are members of the Kuiper belt. Comparisons with numerical integrations (Duncan *et al.* 1995) show that their orbits are dynamically stable for the age of the solar system. The discovery of these 100–200 KM-sized objects proved the Kuiper belt is populated. It did not, however, provide the observational link to show that the Kuiper belt is the major source of the short-period comets because comets are so much smaller. Here we present HST/WFPC2 observations showing there is a large population of Halley-sized objects (radii $\sim$ 10 km) in this region.

2. Observations and Reductions

On 21.7–23.0 August 1994 UT, we obtained thirty-four exposures of a field on the ecliptic near morning quadrature with the "Wide V" filter on HST/WFPC2. Each exposure was 500–600 sec, for a total integration time of 5 hours. The observations were of a single field of 4 arcmin^2 centered at R.A.= 3 41 20, Dec = +19 34.7 (equinox 2000.0). This field was chosen because it was along the ecliptic and prior observations had shown that it contained very few stars and galaxies, which helped minimize confusion from background objects. Thirty hours elapsed from the start of the first exposure to the end of the last. For an outer solar system body observed at quadrature, the Earth's parallactic motion is near zero so that any apparent motion of the body is attributable to the body's orbit. For a body in the Kuiper belt the orbital motion is $\lesssim$1 arcsec hr^{-1}. With the plate scale of the WF chips, this orbital motion is equal to $\lesssim$10 pixels hr^{-1}, $\sim$ 1 pixel in each ten minute exposure, or a total of up to 300 pixels in 30 hours.

In principle, one could inspect a very deep exposure to identify faint trails in the Kuiper belt. However, each WFPC2 frame is littered with hundreds of radiation events. Some appear as single pixels or clusters of pixels; others appear as streaks. It was necessary to remove these prior to searching for Kuiper belt objects. Standard techniques for removing radiation events employ a median sum of many images, and rely on the concept that real objects remain fixed relative to each other, but radiation events appear in random pixels. Unfortunately, the objects we are searching for move relative to background stars and galaxies, and would be removed by these standard methods. In addition to these difficulties, we also needed to remove from our images any objects that do *not* move in the fields as a function of time. To solve both these problems we adopted the following strategy. We produced a median sum of all 34 exposures. This left a high signal/noise image with all of the stars and galaxies but with no Kuiper belt objects and no radiation signatures. Then, this median sum image was normalized and subtracted from each of the individual exposures. At this point, we had 34 images with just radiation events, moving objects, and noise.

The next step was to combine the images so that only the Kuiper belt objects remained. First, we shifted the images so that a Kuiper belt object appeared in the same pixel in all of the frames. To accomplish this, we specified various trial orbits as described in detail in the next section. For any orbit, one can compute the drift rate of an object moving on that orbit during the interval of our observations. We shifted each image to compensate for the drift rate to produce 34 images which were all co-aligned to one of the images for the desired orbit. Then we combined the shifted images into a median sum so that a Kuiper belt object with the predicted drift rate would be in the same pixel for each shifted image, and thus would remain in the sum. In contrast, random radiation events would be unlikely to co-align. Indeed, if a particular physical pixel of the CCD were always high, that pixel would not create a detectable signal in the median sum since it would be shifted into different places. This process also removed main belt asteroids which traversed our field since they appear as streaks.

After computing the image medians, we found by inspection that there were no obvious bright objects in our field. Therefore, we developed an automatic search routine to examine each of the summed images for faint objects. For each pixel in the image, we computed the average signal for a five pixel pattern (a "plus") centered on the pixel. This was compared with the local background which was computed as the mean of a 15×15 pixel box centered on the pixel under study. If the plus average was higher than at least 1.5σ of the background, this pixel was flagged for further investigation. Our results are not sensitive to the choice of the 1.5σ limit since our ultimate detection limit was set by our further processing and calibration.

We needed to develop a mechanism for determining which of the resultant "objects" were real and which were just coincidental alignments of noise. This goal was complicated by the fact that the PSF of a star in our frames was only 1.3 pixels FWHM, so that it is not possible to distinguish definitely between noise spikes and real objects by the width of their images. Thus, we adopted the following strategy. From the 34 individual exposures we created 6 images, each consisting of half of the exposures. The first of the six contains the first seventeen exposures. The second contains the last seventeen. The third and fourth contain the even and odd exposures, respectively. The fifth and sixth images contain $1, 2, 3,\ 7, 8, 9,\ \ldots$ and $4, 5, 6,\ 10, 11, 12,\ \ldots$, respectively. We require that something show up in the same pixel in at least four of these six images for it to be retained for further statistical analysis. As with our choice of σ above, the condition that a candidate be in at least four (as opposed to three or five) images did not significantly affect our results. Something in fewer than four images would have been rejected later by the statistical analysis.

In order to understand our detection threshold, we ran tests with artificial data. Using the calibration supplied by STScI, we implanted objects of known magnitudes from V=23 to 29.5 into the original 34 exposures. Each object was implanted at a different pixel in each exposure to simulate it moving on a Kuiper belt orbit. We then processed these images using our standard reduction procedure as described above. We found that the automatic search was complete to V=27.7. By V=28.6, this search detected only 50% of the artificial objects. No artificial objects fainter than V=29.5 were detected. To be conservative, we defined the "limiting magnitude" of our search as V=28.6, which corresponds to a detection probability of 50%. (Hainaut *et al.* (1994) ran a similar test on their NTT data and concluded that their detection threshold was at the 90% probability level. Since they were searching for specific objects rather than comparing with a control sample, they could not allow for false detections in their analysis; our statistical approach does not prohibit them.)

With these artificial data, we were thereby able to calibrate the magnitudes of the real objects which we detected.

When searching for objects so close to the detection threshold, it is possible that coincidental alignments of noise will occasionally occur. To quantify how many of our "detections" were likely to be false alarms, we proceeded as follows. To understand the noise properties, we shifted and co-added images using orbits which were non-viable Kuiper belt orbits, such as retrograde orbits. We do not expect such orbits to be populated because the Kuiper belt is a disk. For every Kuiper belt orbit for which we produced the six sums described above, we also produced the comparable six sums for the same orbit but with the velocity of the object reversed. These were then searched with our automatic search routine in the same manner as the true orbit images. The results of these searches were analyzed in the same statistical manner as the true orbits. There was no difference in the processing of the prograde and retrograde orbits other than the sign of the velocity, thus nothing which we did should produce systematic differences.

3. Results and Analysis

Because an object in the Kuiper belt would orbit the Sun once every ~ 250 years but our observations only span 30 hours, we cannot uniquely constrain the orbit of any particular object. However, our reduction process produces a distribution of objects as a function of various orbital parameters. As noted above, we must specify the orbit of the objects that we are searching for before we begin our reduction procedures. The ability to detect an object is strongly sensitive to our choice of the assumed orbit, and thus a complete search of the images requires a very fine grid in orbital element space. The only "observables" of the orbit are its drift rate with respect to the background stars ($\dot{\theta}$) and the angle the orbit makes with the ecliptic (ϕ). We found that in order to find all the objects and yet not find an object more than once, a grid with a resolution of $\sim 0.1\,\mathrm{arcsec\ hr^{-1}}$ in $\dot{\theta}$ and $\sim 1^\circ$ in ϕ is required. In the long run, we plan to study ~ 500 possible prograde orbits. So far, we have studied 154 prograde orbits and their 154 retrograde counterparts.

We present the results of a search for objects with $\dot{\theta} \in [0.73, 1.16]\,\mathrm{arcsec\ hr^{-1}}$ and $\phi \in [0, 30.3]$ deg. We chose this $\dot{\theta}$ range because it is the drift rate of objects at perihelion in Neptune's 2:3 mean motion resonance ($a = 39.4\,\mathrm{AU}$) for orbital eccentricities of 0.1 to 0.3. We interpret the drift rates in terms of objects in this resonance for two reasons. First, the 2:3 mean motion resonance with Neptune is known to be populated. (Pluto is in this resonance, as are at least 2 and perhaps as many as 8 of the 24 known 100-200 KM-sized Kuiper belt objects; Marsden 1994, 1995). Second, objects in these orbits have the smallest perihelion distances in the stable Kuiper belt (Duncan *et al.* 1995, Morbidelli *et al.* 1995) and thus, an object of a given size appears brightest in these orbits. We note, however, that the drift rates we studied are consistent with many other orbits which are not in a 2:3 mean motion resonance with Neptune. For example, our range in $\dot{\theta}$ is consistent with circular orbits with semi-major axis, $\sim 25 < a < 32$ AU, and with objects at perihelia in parabolic orbits with perihelion distances between ~ 32 AU and ~ 43 AU. Indeed, with our choices of $\dot{\theta}$ we will find objects that are in orbits with $a \in [30, 40]$ AU and with moderate eccentricity, over most of their orbital phase. (Orbits beyond this range of semimajor axis comprise the remainder of the 500 orbits in our survey. The results of that study will be presented elsewhere.) It is possible that some of the objects we found are Centaurs near aphelion. However, since the density of Centaurs is orders of magnitude smaller than the expected Kuiper belt density (Levison & Duncan 1995), it is unlikely we would find a Centaur in our small field of view.

Since we are observing on the ecliptic, every object we discover must be passing through one of its nodes. Thus the relationship between inclination, i, and ϕ is simply $i = |\phi - \phi_E|$, where $\phi_E = 0.3°$ is a small correction due to the shift from heliocentric to geocentric coordinates. For every value of i there are two values of ϕ, depending on which node the object is at. We studied orbits with $\phi \in [0, 30.3]$, which implies we are sensitive to half the orbits with $i < 30°$ (we have not yet searched $\phi < 0$ orbits).

On average, we found approximately 0.5 candidate objects per orbit studied. To demonstrate that we found real objects and to determine their physical and dynamical characteristics, we combined the results of all of our orbits with $i < 12°$ to form a statistical sample. Our analysis found 53 candidate objects in the prograde orbit set, but only 24 in the retrograde orbit set[2]. A χ^2 analysis shows that the probability that these numbers are drawn from the same population is 9.5×10^{-4}. There is no significant excess of candidates in our prograde sample for $i > 12°$.

Figure 1 shows the magnitude distribution of candidate objects in the prograde and retrograde sets of orbits. Notice the prograde candidates typically outnumber the retrograde candidates in the bins brighter than our limiting magnitude, and the brightest candidate discovered is in the prograde data set. Visual inspection of several of the brightest prograde candidates shows that they are indeed detected in each frame and that they appear stellar, confirming that they are very likely real. We conclude that we are seeing excess candidates in the prograde orbit set at >99.9% ($1 - 9.5 \times 10^{-4}$) confidence level. Since the prograde

[2]These numbers differ from those reported in IAUC 6163 because the present analysis is restricted to objects with $V \leq 28.1$; fainter objects were included in the Circular.

and retrograde orbit sets were reduced in exactly the same way and there should not be any systematic difference in the noise characteristics, we conclude that we are seeing a population of objects in the outer solar system that preferentially populates prograde orbits.

The slope in the distribution shown in Figure 1 may appear surprisingly steep. However, the limiting magnitude of our survey is close to the magnitude of the brightest object found in our field. In such cases a steep slope in the observed magitude distribution is inevitable, independent of the intrinsic slope of the distribution.

We also compare the prograde and retrograde candidates by looking at their inclination distributions. In Figure 2, we bin our results so that each plotted point contains a sum of the data for all eccentricities at a given prograde inclination. As a comparison, the dotted line shows the mean of the number of candidates in the retrograde orbits found in all the inclination bins (the individual retrograde orbit values are shown as asterisks). Thus, the dotted line can be viewed as the zero point. Each prograde and retrograde bin includes eleven different eccentricity values. The figure shows a steady decrease in the number of objects as a function of i. The over abundance of objects in the prograde orbits disappears for inclinations above $\sim 15°$. Interestingly, we see a strong, statistically significant, peak in the inclination distribution at about $3°$. Most of the offset of the peak from $0°$ can be attributed to the difference between ecliptic and invariable plane inclinations and the low probability of very small inclinations (which require orbit poles in small areas of the celestial sphere; Marsden priv. comm.).

The inclination distribution shown in Figure 2 adds evidence that the excess objects detected in the prograde orbits are indeed in the Kuiper belt. As discussed in §1, before the discovery of 1992QB1 by Luu & Jewitt in 1992, the primary argument in support of the existence of the Kuiper belt was the theoretical argument that it was required to be a flattened reservoir in order to explain the low inclination distribution of the short-period comets (Fernández 1980; Quinn *et al.* 1990). Our observations show that the population that we are detecting is made up of low inclination objects, consistent with models of the Kuiper belt and all 24 known 100–200 KM objects in the belt.

Finally, it is possible to estimate the size distribution of the objects we found. To be conservative we only include objects brighter than 28.6. The first step in determining this distribution is to remove observational biases. There are four such biases that must be removed: (1) We first removed contamination due to false detections. To accomplish this, we calculated the probability that a candidate was real as a function of magnitude, $p_r(V)$, from the histograms shown in Figure 1: $p_r(V) = [N_{pro}(V) - N_{retro}(V)] / N_{pro}(V)$. In order to smooth out this function, we fit a line to the resulting relationship. (2) We corrected for the fact that our observations were only complete to $V = 27.7$, but we were seeing some objects down to $V \sim 29.0$. We calculated the probability that an object was discovered as a function of V magnitude, $p_d(V)$. We took $p_d(V) = 1$ for $V < 27.7$ and assumed that it linearly decreased as V increased so that at $V = 28.6$, $p_d(V) = 0.5$. A linear relationship is consistent with the results of the tests we performed using artificial objects, as discussed in §2. (3) We corrected for the fact that large objects could be seen at greater distances from the Sun than small objects by calculating the fraction, f_V, of the volume of space that we searched (as defined by our choice of orbits) in which an object of a particular radius would actually have been visible to us. The inner edge of the volume was taken to be 25.5 AU, corresponding to the perihelion distance of an object in Neptune's 2:3 mean motion resonances with $e = 0.3$. The outer edge of the volume was taken to be 35.5 AU, corresponding to the perihelion distance of an object with the same semi-major axis but with $e = 0.1$. We performed this calculation assuming a limiting magnitude of $V = 28.6$. And (4) we corrected for the fact that the effective size of our field is a function of $\dot{\theta}$ and ϕ. This can be seen by recognizing that the larger the drift rate, the more we had to shift the frames to compensate for the orbits of the body, thus the smaller the effective field. We determined by visual inspection the fraction of the field, f_F, over which we could find objects. For each of our prograde candidates, we calculated its current heliocentric distance, r, under the assumption that it was in Neptune's 2:3 mean motion resonance and was at perihelion. We then calculated its radius, R, assuming an albedo of 0.04. We assigned a weight to the candidate, $w = p_r/(p_d\, f_V\, f_F)$. This weight is an estimate of this object's contribution to the size distribution of real Kuiper belt objects.

The solid curve in Figure 3 shows the size distribution of our candidate objects as derived using the above procedure. Note that under the assumption of an albedo of 4%, we found objects as small as 5 KM in radius! Also shown in Figure 3 are two hypothetical size distributions of the form $n(R)dR \propto R^{-b}\, dR$. A distribution with $b = 3$ is believed to be a reasonable representation of the size distribution of the known short-period comets (Shoemaker & Wolfe 1982). A distribution with $b \sim 5$ is required for larger objects in the Kuiper belt in order to reconcile the number of comets believed to be there and the number of known 100–200 KM objects (Duncan *et al.* 1995). Although there are significant uncertainties in our derived size distribution due to the small number of objects detected, as well as to inaccuracies in determining the magnitudes of the objects and their exact heliocentric distances, it appears there is a reasonable size distribution for our objects.

4. Conclusion

We have used HST's WFPC2 to deduce that there are a substantial number of Halley-sized objects in a disk-like structure in the region near and beyond the orbit of

Neptune. We found 29 objects with radii ranging from 5 to 10 KM (4% albedo) in the orbits discussed in §3. Our observations imply there are $\sim 25,000$ objects degree^{-2} brighter than $V = 28.6$. Thus, there are $> 2 \times 10^8$ comets in this size range in orbits similar to the ones we have studied here. Combining this number with the size distribution shown in Figure 3 and assuming a density of 0.5 GM CM^{-3} implies a total of 0.02 Earth masses of 5–10 KM comets in *this region* of the Kuiper belt. We note that the derived radii are uncertain to a factor of a few and the density of comets is highly uncertain. Therefore, it is possible that the mass in this region of the Kuiper belt differs from that quoted here by as much as an order of magnitude.

The observations presented here represent the first reported detections of objects the size of typical short-period comets *in their native reservoir*. Their detection shows that the idea is indeed correct that a significant number of planetesimals extends the solar system past the region of the planets. These objects appear to be confined to a moderate-thickness disk near the plane of the ecliptic, as is necessary if these objects are the source of most of the short-period comets. For the first time, one can point to a definitive region of the solar nebula for the origin of short-period comets.

We thank A. Whipple, W. Cochran, J. Bally, B. Marsden, S. Tremaine, and P. Weissman for helpful discussions. Support for this work was provided by NASA through GO-5312.01-93A from the Space Telescope Science Institute which is operated by the Association of Universities for Research in Astronomy, Inc., under NASA NAS5-26555.

REFERENCES

Duncan, M, Levison, H., & Budd, M. 1995. AJ, in press

Duncan, M., Quinn, T., & Tremaine, S. 1988, ApJ, 328, L69

Edgeworth, K.E. 1949. MNRAS, 109, 600

Everhart, E. 1972, ApJ, 10, L131

Everhart, E. 1977, in *Comets–Asteroids–Meteorites,* ed. A.H. Delsemme, (Ohio: University of Toledo Press), 99

Fernández, J. A. 1980, MNRAS, 192, 481

Hainaut, O., West, R. M., Smette, A. & Marsden, B. G. 1994. A&A 289,311

Holman, M., & Wisdom, J. 1993. AJ, 105, 1987

Jewitt D. & Luu, J. 1992. IAU Circulars, 5611

Jewitt D., & Luu, J. 1995. AJ, 109, 1867.

Kuiper, G. P. 1951. In *Astrophysics: A Topical Symposium*, ed. J.A. Hynek, (New York: McGraw Hill), 357

Levison, H. & Duncan, M. 1993. ApJ, 406, L35

Levison, H. & Duncan, M. 1995. In preparation

Marsden, B. G. 1994. IAU Circulars 5983

Marsden, B. G. 1995. MPEC 1995-C17

Morbidelli, A., Thomas, F. & Moons, M. 1995. Icarus submitted

Newton, H. 1893, *Mem. Natl. Acad. Sci.*, 6, 7

Quinn, T., Tremaine, S., & Duncan (1990). ApJ, 355, 667.

Shoemaker, E., & Wolfe, R. 1982 in *Satellites of Jupiter* (ed. Morrison, D.), 277.

Stern, S.A. 1995, To appear in 'Completing the Inventory of the Solar System', ed. E. Bowell. (ASP Conference Series)

Weissman, P. 1995. *Ann. Rev. Astron. Astrophy.* 33, 327

5. Figure Captions

Figure 1 — A histogram of the number of Kuiper belt candidates we found as a function of V magnitude. The solid green and dotted red curves refer to candidates discovered in our prograde and retrograde orbit sets, respectively. The dashed line shows our "limiting" magnitude (*i.e.* at which the detection probability is 0.5) at $V = 28.6$.

Figure 2 — The solid dots show the number of candidate objects found in our prograde orbit set as a function of their orbital inclination; the asterisks show the candidates from our control sample. The dotted horizontal line shows the mean number of candidates found in the retrograde frames and can be interpreted as the number of false detections per inclination bin. Note the significant number of excess candidates at low inclination, but the excess becomes insignificant for $i \gtrsim 15°$.

Figure 3 — The size distribution of our excess candidate objects is shown in the form of a histogram (solid curve) of the number of objects as a function of radii, R. Also shown are two hypothetical differential size distributions of the form $n(R)dR \propto R^{-b}\,dR$ with $b = 3$ (dotted curve) and $b = 5$ (dashed curve), respectively. The total area under the each curve is normalized to 1.

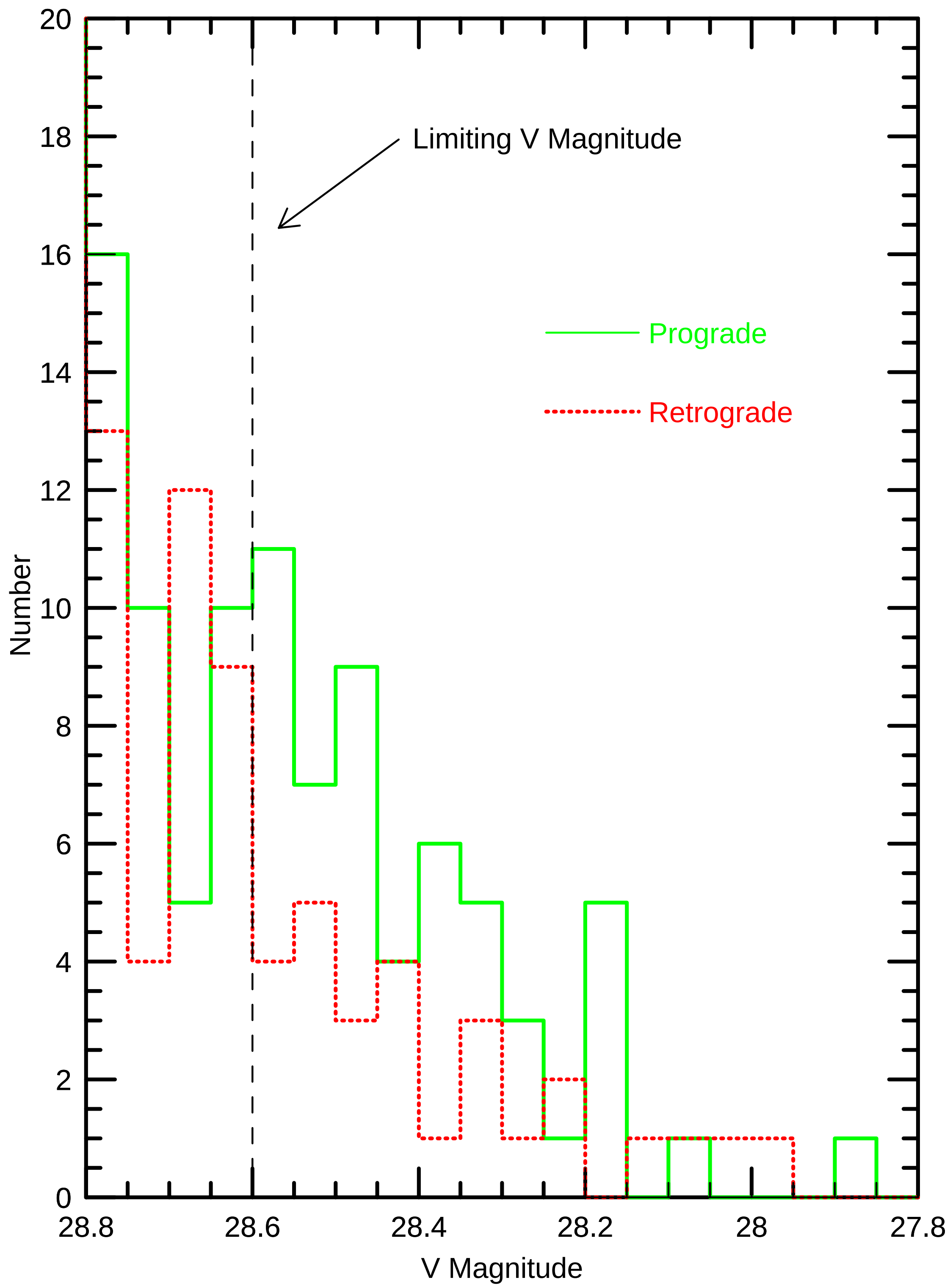
Limiting V Magnitude
Prograde
Retrograde
Number
V Magnitude
0
2
4
6
8
10
12
14
16
18
20
28.8
28.6
28.4
28.2
28
27.8

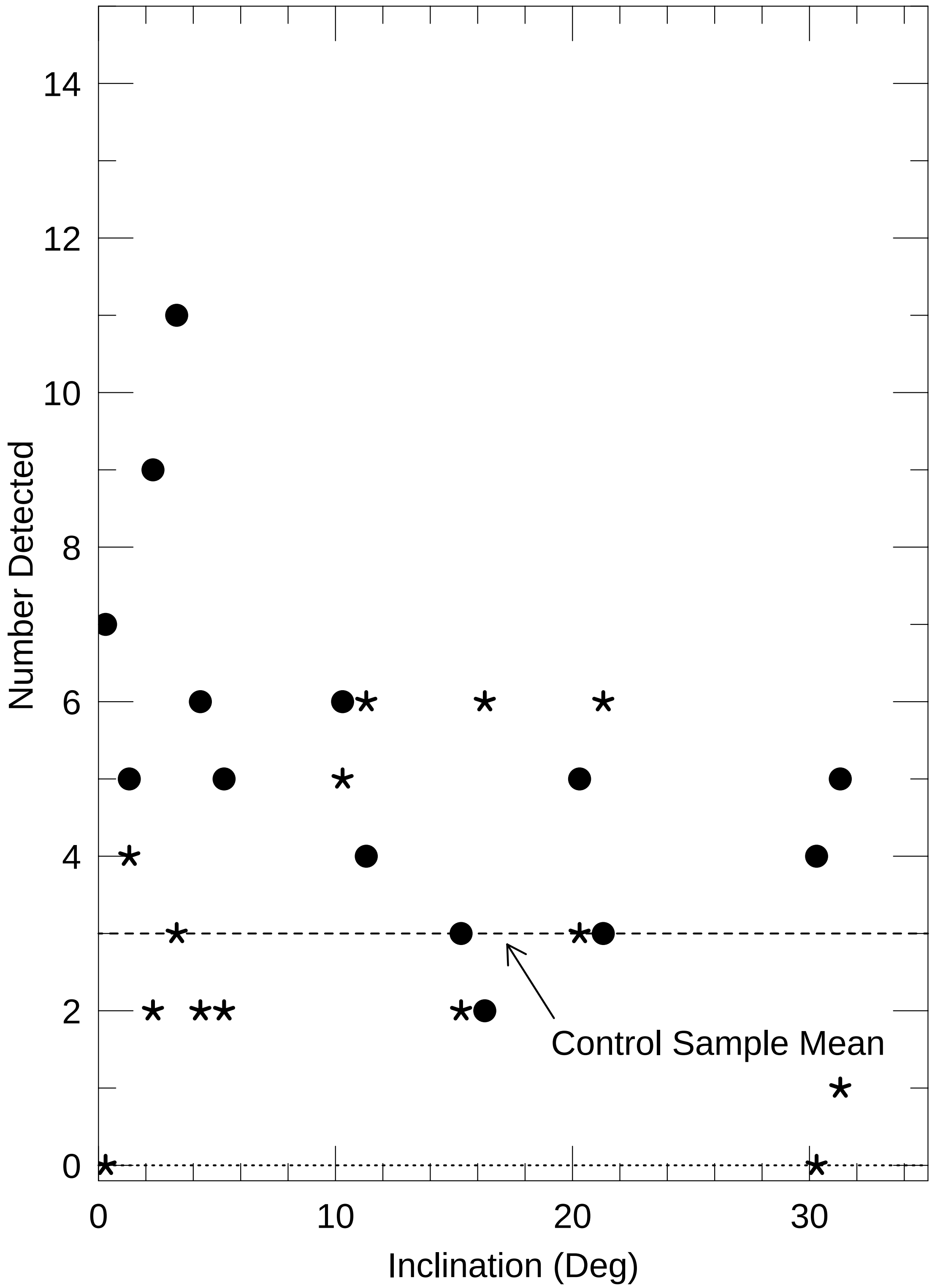
14
12
10
8
6
4
2
0
Number Detected
0
10
20
30
Inclination (Deg)
Control Sample Mean

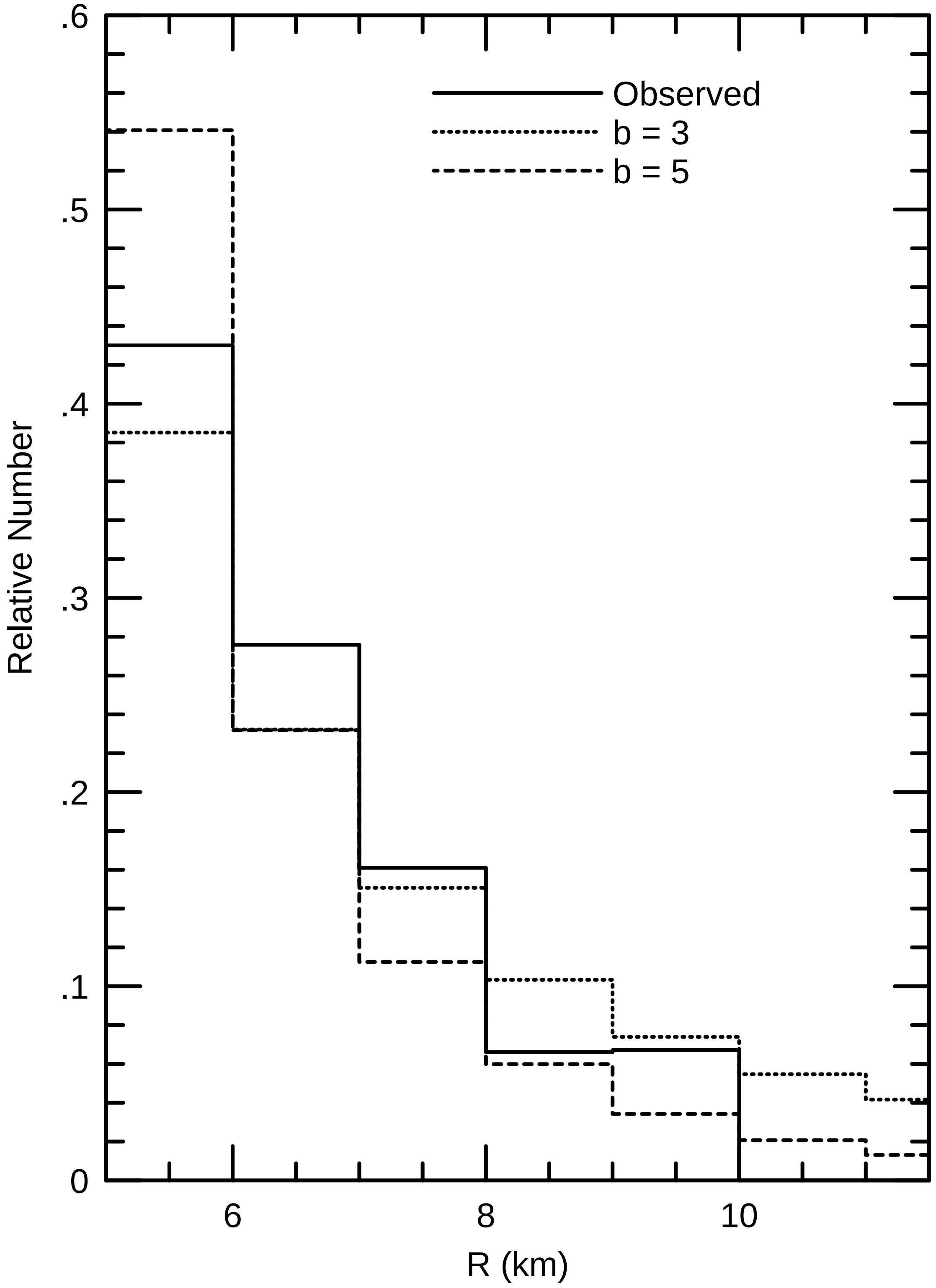
Observed
b = 3
b = 5
Relative Number
R (km)
0
.1
.2
.3
.4
.5
.6
6
8
10